J. Fluid Mech. (1994), *vol.* 265, *pp.* 217–244

The spin-up from rest of a fluid-filled torus

By F. N. MADDEN AND T. MULLIN

Department of Atmospheric, Oceanic and Planetary Physics, Clarendon Laboratory, Oxford OX1 3PU, UK

(Received 9 September 1992 and in revised form 4 October 1993)

We present the results of an experimental and numerical study of the spin-up from rest to solid-body rotation of a fluid-filled torus. In separate experiments, the rotation rate of the container is suddenly increased to a fixed value and the final rotation rate is used to define a non-dimensionalized control parameter, C. At low values of C, the observed flows during the transient phase are axisymmetric and spin-up is achieved through viscous diffusion. This in turn is followed by significant secondary flow and the appearance of 'fronts' as C is increased. During the transient phase the fluid motion near the inner wall of the container is dynamically unstable according to Rayleigh's criterion. Thus at higher values of C wave-like structures break the axisymmetry, non-uniqueness in the details of the process is found and finally, an inner wall instability is observed directly. A plot of the spin-up time versus C shows breaks in the slope at transition points between each of the above dynamical regimes but the overall trend is found to be insensitive to the details of the fluid motion. Further elucidation of the dynamical processes is provided by a novel variant of the now standard phase-space reconstruction techniques. The results show a systematic splitting of the phase paths as C is increased.

Finally, in the complementary numerical study, the time-dependent Navier–Stokes equations are solved for axisymmetric flows. Here, the flow is computed using a velocity–streamfunction–vorticity formulation in a two-dimensional plane with a velocity component normal to this plane. The quantitative and qualitative agreement between the numerical and experimental results is excellent for moderate values of the dynamical control parameter C.

1. Introduction

Laboratory studies of spin-up problems are usually concerned with hydrodynamic motions generated by a change in the rotation rate of the fluid's containing vessel. In our case, we used experimental and numerical techniques to study the situation where a fluid is spun-up from rest when an axisymmetric container's rotational speed is increased from zero to some closely controlled final value. The spin-up process can be considered as the transient between two well-defined dynamical states – those of rest and rigid-body rotation. The geometry is of a fluid-filled torus which is mounted as if it were a bicycle wheel spinning in the usual way on its central axis. When the final rotation rate is small it is found that the spin-up takes place through the diffusion of vorticity from the container walls. At high rotation rates, however, the fluid motion near the inner wall of the container during the transient phase will be hydrodynamically unstable according to the Rayleigh criterion as the fluid circulation will decrease outwards away from the axis of rotation. Therefore, one might expect to see instabilities develop in that region, above some critical rotation rate, which may then

grow and lead to a transient formation of turbulence. It might be anticipated that this feature will have a significant effect on the spin-up process since turbulence usually enhances the transport of vorticity. However, in the present case, the final state is solid-body rotation and thus the turbulence itself must decay. Thus there is a subtle interplay between the creation and decay of turbulent motion as will be discussed later. More importantly, it is in the range between these two extremes where most of the interesting behaviour takes place and the combination of numerical and experimental work to be presented below has revealed some novel dynamical processes.

The majority of previous research on spin-up problems has been concerned with processes where the fluid motion is hydrodynamically stable and thus considerable analytical and experimental progress can be made. Greenspan & Howard (1963) analysed spin-up processes of this type using linear methods and identified three distinct phases. These are the formation of Ekman boundary layers, secondary flow within the body of the fluid and finally viscous decay of residual motion. Greenspan & Howard also used the linear theory to predict a characteristic spin-up time for two cylindrical geometries which are bounded in the first case by a flat disk and in the second by a conical section where both the disk and conic sections rotate with the cylinder walls. In each case, they confirmed the theoretical prediction by experiment. A great deal of the early work in this subject area is discussed in the book by Greenspan (1968) where details of the processes involved are also given. A more up to date and extensive review of work on spin-up processes is to be found in Benton & Clarke (1974).

More recent work on the axisymmetric spin-up of fluid in cylinders has been carried out by Watkins & Hussey (1977). They considered both experimentally and numerically the spin-up from rest of a fluid in a closed cylindrical container and found good agreement between their numerical calculations and their experimental observations over a wide range of control parameters. Ibrani & Dwyer (1987) investigated the spin-up of flows in both cylindrical and spherical geometries using numerical techniques. In each case they found the presence of an inertial oscillation, which is in agreement with both linear and weakly nonlinear theory as outlined by Greenspan (1968). These inertial oscillations are also found in the present experimental and numerical results, which are discussed in detail in §4.

Pertinent early numerical calculations on an unstable spin-up process were carried out by Pearson (1967) who studied the axisymmetric time-dependent flow between coaxial rotating spheres. The spheres were free to rotate independently about a common pole and all of the solutions were constrained to be not only axisymmetric but also symmetric about the equatorial plane. In one of the situations considered both spheres corotate with a given angular velocity. This velocity is suddenly increased and results in the spin-up of the contained fluid. Initially, when the rotation rate of the container is increased, fluid near the inner and outer spheres gains angular momentum through the action of viscosity in boundary layers.

If we consider a region near the inner sphere in the above problem it can be seen that the rate of change of angular velocity with radial distance from the rotation axis is negative during the initial phase of the transient. Thus one might expect to find transient instabilities akin to those found between differentially rotating spheres if the velocity gradient is large enough. (An extensive review of the flow between rotating spheres is given by Yavorskaya *et al.* 1980.) This possibility was not discussed by Pearson but it might be expected to play a significant role in the spin-up process at large rotation rates as the instability may grow and lead to three-dimensional effects. We chose to study transient instabilities of the above type in a toroidal domain because it

not only permits systematic investigation but also combines aspects of symmetry with practicability. The geometry can be considered as a long pipe of circular cross-section which is bent into a circle so that its ends meet. This is thus a novel domain for spin-up problems since it is doubly connected.

The transient flow in the torus has some features in common with pressure-driven flows in curved pipes – the so-called 'Dean problem' (Dean 1928). Indeed, theoretical analyses of coiled or curved pipe flows are often made using a toroidal flow domain which is then approximated experimentally by considering the case of small pitch, i.e. the depth through which the pipe is coiled. A review of flows in curved pipes is given by Berger, Talbot & Yao (1983) and here we will only comment on those features that are directly relevant to flow in toroidal domains.

Early analytical work on pressure-driven flows in curved pipes was performed by Dean (1928) who showed that when the radius of the pipe is small compared with the radius of curvature (i.e. a narrow pipe loosely coiled), the system is characterized by a single controlling parameter which later came to be called the Dean number. The steady flow consists of an axial component along the pipe and a secondary circulation which is in the cross-sectional plane of the pipe. When the pipe is of circular cross-section the secondary flow consists of two counter-rotating vortices which are aligned so that the flow through the cross-section centre is directed away from the curvature axis.

More recently, Munson (1976) has shown that in the case of a slowly oscillating torus, the sense of rotation of the secondary vortices is in the opposite direction to that for the pressure-driven flow of the Dean problem. This difference can be understood in terms of the centrifugal force which gives rise to the secondary flow. In the pressure-driven flow through a curved pipe the no-slip condition at the wall imposes a distribution of the axial velocity component within the cross-section of the pipe. This distribution peaks near the centre of the pipe and so the centrifugal force acting on the fluid at this point is greater than that acting on the fluid near the wall at a similar distance from the curvature axis. This imbalance leads to the observed circulation pattern. In the work of Munson (1976), the fluid with greater angular velocity is adjacent to the moving walls. Thus the imbalance in centrifugal force works in the opposite sense and the rotating vortices produce a stream in the cross-section centre towards the rotation axis. It is therefore to be expected that similar secondary flow effects to those observed by Munson will arise in the transient process studied here and since they will act to transport vorticity from the container walls then they will play a crucial role in the spin-up of the fluid.

Further relevant work on time-dependent phenomena in curved pipe flows is to be found in Lyne (1970) who reported the presence of a four-vortex secondary flow in the high-frequency limit of a flow field driven by an applied oscillatory pressure gradient. His analysis consisted of a boundary-layer approximation for the flow near the wall which was matched to an inviscid core in the interior. The four-vortex state was also observed in experiments by Lyne and has subsequently been confirmed by Bertelsen & Thorsen (1982). This state has also been observed by Munson in the oscillating torus problem. In the present study, we also find a four-vortex flow in the numerical calculations of sharp transients but it has not been observed in the experiments since other complications arise in the relevant parameter ranges.

Another area of great interest in curved pipe flows is that of suddenly accelerated flow. Cowley, Van Dommelen & Lam (1990) showed that impulsively started flow through a stationary curved pipe is a process where boundary-layer collision and unsteady separation can occur in the limit of high Dean number. Lam (1988) provides

a more extensive account of this phenomenon and also includes calculations of the flow due to the impulsive rotation of a curved pipe about its curvature axis. The situation in the latter case is best considered in the cross-sectional plane of the pipe and flow development proceeds as follows. The pipe is impulsively started and boundary layers begin to form. Fluid in these layers is forced outwards along the walls and the two streams collide at the point furthest from the rotational axis. The collision causes the boundary layer to grow rapidly in thickness and then to separate. At this point the calculations of Lam (1988) cease as a singularity is encountered. Unfortunately, we were not able to investigate these phenomena directly as it proved to be experimentally impossible to produce a sharp enough impulsive start. However, some of the results detailed below seem to support the presence of collision and growth processes.

As discussed above, the spin-up process can be considered as the evolution of the flow from one uniquely defined dynamical state (rest) to another (solid-body rotation). In dynamical-systems parlance we could usefully consider this procedure as the evolution from one fixed point in phase space to another along a trajectory linking the two points. With this view it is interesting to inquire whether the path is always unique over the entire parameter range or whether there is any evidence for bifurcation phenomena. The investigation of such bifurcation phenomena has been the subject of intense research in recent years and a great deal of success has been achieved in the elucidation of complex bifurcation sequences for some fluid systems, e.g. Taylor–Couette flow. In these systems the interaction of qualitatively different types of bifurcations has been shown to give rise to non-trivial low-dimensional dynamical behaviour (including chaos) and enables a link to be formed between ideas of dynamical systems and the Navier–Stokes equations. A review of finite-dimensional dynamics in Taylor–Couette flow is given by Mullin (1993).

We show in §4 that there is considerable merit in considering the spin-up process in terms of ideas from dynamical-systems theory using an adaptation of the method of Broomhead & King (1986) for reconstructing the trajectories from a measured velocity time series. We discuss in §3 a novel method for averaging the trajectories of many individual spin-up experiments so that a comparison can be made of the dynamics of many different runs, each of which is performed at the same parameter values.

The rest of the paper is organized in the following way. We present in §2 the geometry and techniques used to numerically study the spin-up processes of the flow. In §3 we give details of the experimental methods and we describe an adaptation of the method of phase-space reconstruction from time series used to produce 'averaged' phase portraits, mentioned above. A comparison between experimental and numerical results is presented in §4, and finally some conclusions are given in §5.

2. Numerical study

Details of the geometry and coordinate system employed are described in this section. The equations of motion are then presented and the finite-difference numerical techniques used in the solution of the discretized equations are discussed.

2.1. *Geometry*

The coordinate system used is shown schematically in figure 1. The distance OO' is denoted by R, and the plane angle ϕ gives the position of O' on the circle of radius R. The radial direction r is defined by $O'P$, and this line lies in the plane containing O, which is orthogonal to that containing ϕ. The angular coordinate θ is defined by $OO'P$.

In this coordinate system, a solid torus is defined by R, $0 \leqslant r \leqslant a$ (where $a < R$),

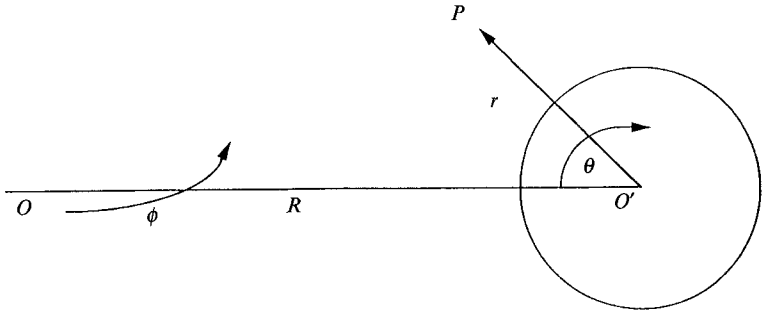

FIGURE 1. Toroidal coordinate system used in the numerical calculations.

$0 \leqslant \theta \leqslant 2\pi$ and $0 \leqslant \phi \leqslant 2\pi$. This gives a torus with major and minor radii R and a respectively.

A point $\boldsymbol{P}$ is specified by (r, θ, ϕ) and $\mathrm{d}\boldsymbol{P}$ is given by

$$\mathrm{d}\boldsymbol{P} = \mathrm{d}r\boldsymbol{r} + r\,\mathrm{d}\theta\boldsymbol{\theta} + r^*\,\mathrm{d}\phi\boldsymbol{\phi} \tag{1}$$

where $\mathrm{d}r$, $\mathrm{d}\theta$, and $\mathrm{d}\phi$ indicate the changes in those quantities and r^* is given by

$$r^* = R - r\cos\theta. \tag{2}$$

Equations (1) and (2) define the scale factors for this coordinate system. These are used, together with their derivatives, to define the vector operators (e.g. ∇^2 etc.) required for the Navier–Stokes equations (see for example Batchelor 1967, Appendix 2).

The coordinate system as defined above contains a singularity at $r = 0$, in factors of the form $1/r$. This singularity is avoided in the numerical approximation by ensuring that a grid point does not lie exactly on the point defined by $r = 0$.

2.2. *Equations, non-dimensionalization and boundary conditions*

The Navier–Stokes equations expressed in the above toroidal coordinate system are recast in a non-dimensional form by rescaling the variables and coordinates as follows:

$$r = \alpha r_n, \quad R = \alpha R_n, \quad r^* = \alpha(R_n - r_n\cos\theta) = \alpha r_n^*,$$
$$\theta = \theta_n, \quad \phi = \phi_n,$$
$$\boldsymbol{v} = \beta\boldsymbol{v}_n, \quad t = (\alpha/\beta)\,t_n, \quad p = \rho\beta^2 p_n.$$

Here α is taken as the radius of the 'pipe' cross-section. The scaling parameter β is taken to be the velocity in the ϕ-direction at the point $r = 0$, i.e. β is equal to R multiplied by the rotation rate. The subscript n indicates the non-dimensional variables. With this rescaling, the Navier–Stokes equations have the following form:

$$\frac{\partial \boldsymbol{v}_n}{\partial t_n} + (\boldsymbol{v}_n \cdot \boldsymbol{\nabla}_n)\,\boldsymbol{v}_n = -\boldsymbol{\nabla}_n p_n + \frac{1}{C}\nabla_n^2 \boldsymbol{v}_n. \tag{3}$$

The velocity is also subject to the usual continuity constraint

$$\boldsymbol{\nabla}_n \cdot \boldsymbol{v}_n = 0.$$

In the following discussion, the subscript n will be dropped. Consequently, velocities, etc. will be assumed to be non-dimensional unless explicitly stated as otherwise.

The parameter C is similar in form to a Reynolds number and is defined as

$$C = \alpha\beta/\nu,$$

with ν being the kinematic viscosity. Accordingly, the product of toroidal radii is implicit in this definition of C. In both the experiment and the numerical calculations the radius ratio was fixed at 7.8125:1.

The Reynolds number is usually defined as the single controlling parameter for a given flow. However, in the present problem there are two controlling parameters: the radius ratio and C. In the related problem of the flow through a curved pipe, the Dean number (Dean 1928) is defined as the single controlling parameter in the limit of large radius ratios (e.g. this would apply if $R:a$ in the above coordinate definition is greater than 100:1). In considering the flow through curved ducts Winters (1987) showed that the critical Dean number for a bifurcation point is highly dependent on the radius ratio when the ratio is reduced below 50:1. Therefore, the usual scaling arguments cannot be applied in the type of tightly curved tube used in the present case. However, it is convenient to define the control parameter C in this way to simplify the discussion of the results.

The numerical iteration scheme, which is detailed below, uses a vector stream function, the vorticity $\boldsymbol{\omega}$, and the velocity $\boldsymbol{v}$. The relevant equations are

$$\frac{\partial \boldsymbol{v}}{\partial t} + (\boldsymbol{v}\cdot\boldsymbol{\nabla})\,\boldsymbol{v} = -\boldsymbol{\nabla}p + \frac{1}{C}\nabla^2\boldsymbol{v}, \tag{4}$$

$$\boldsymbol{\omega} = \boldsymbol{\nabla}\wedge\boldsymbol{v}, \tag{5}$$

$$\frac{\partial \boldsymbol{\omega}}{\partial t} + (\boldsymbol{v}\cdot\boldsymbol{\nabla})\,\boldsymbol{\omega} = (\boldsymbol{\omega}\cdot\boldsymbol{\nabla})\,\boldsymbol{v} + \frac{1}{C}\nabla^2\boldsymbol{\omega}, \tag{6}$$

$$\nabla^2\boldsymbol{A} = -\boldsymbol{\omega} + \boldsymbol{\nabla}(\boldsymbol{\nabla}\cdot\boldsymbol{A}), \tag{7}$$

$$\boldsymbol{v} = \boldsymbol{\nabla}\wedge\boldsymbol{A}. \tag{8}$$

Implicit in the numerical method is the assumption that a vector stream function $\boldsymbol{A}$ exists as defined by (7), and this in turn, defines the $\boldsymbol{v}$ in (8). Thus $\boldsymbol{v}$ becomes a valid solution of the non-dimensionalized Navier–Stokes equations and satisfies the continuity constraint and boundary conditions. In addition, an axisymmetry in ϕ is imposed on the solution, i.e. all flow variables are independent of ϕ. This reduces the problem to calculations within (r, θ) – the two-dimensional cross-section – with the third, primary flow component normal to this plane. Thus, $\boldsymbol{v}_\phi$ is independent of pressure, and $\boldsymbol{v}_r$ and $\boldsymbol{v}_\theta$ depend only on $\boldsymbol{A}_\phi$. In addition, $\boldsymbol{A}_\phi$ is only dependent on $\boldsymbol{\omega}_\phi$.

The boundary of the torus is defined by the circle $r = a$, and on this surface the velocity is fixed by the usual no-slip condition. Here the stream function is set to zero and the vorticity is determined by the velocity field and (5). Finally, the nature of the problem we consider eliminates any potential part in the decomposition of $\boldsymbol{v}$ in (8).

2.3. *Numerical solution*

Equations (4)–(8) are solved iteratively in order to calculate the transient flow produced when the initially stationary fluid is set in motion by the impulsive rotation of its toroidal container in the ϕ-direction. Each iteration consists of five steps:

1. equation (4) is used to time step the ϕ-component of velocity;

2. the r- and θ-components of vorticity are calculated using (5);
3. the ϕ-component of vorticity is time stepped using (6);
4. equation (7) is used to define the ϕ-component of the stream function;
5. the r- and θ-components of velocity are calculated using (8).

The whole procedure is then iterated until solid-body rotation has been reached.

Time stepping was performed using the standard alternating direction implicit technique (ADI). A practical method for implementing this technique is discussed by Press *et al.* (1988). The ADI scheme can be considered as a generalization of the Crank–Nicholson method and is second-order accurate in space and time. The nonlinear terms (e.g. $(\boldsymbol{v}\cdot\boldsymbol{\nabla})\boldsymbol{v}$) are treated in an explicit manner.

The ϕ-component of the stream function was calculated by solving (7), which is reduced to a Poisson relationship, where A_ϕ is only dependent on ω_ϕ, when axisymmetry is assumed. We chose to solve this equation by using the standard technique of simultaneous over-relaxation which is also discussed by Press *et al.* (1988).

In the physical process, the fluid is set in motion through the action of boundary layers in the initial stages of the spin-up. Greenspan (1968) provides an estimate for the thickness of the quasi-steady boundary layer in a spin-up process as $(\nu/\omega)^{\frac{1}{2}}$. In the present arrangement, this is equivalent to $(rR/C)^{\frac{1}{2}}$ with $rR = 2000$ mm^2 (r is 16 mm and R is 125 mm).

This estimation provides an Ekman layer of thickness 44.7 mm for $C = 1$, 14.14 mm for $C = 10$, 4.47 mm for $C = 100$ and 1.41 mm for $C = 1000$ which is the upper limit of the range of validity of the numerical results. Thus the thinnest quasi-steady boundary layer to be considered is approximately 8 % of the tube radius and this must be properly resolved on the finite-difference grid for a good representation of the flow field. In practice, at the upper limit of $C = 1000$ there were three grid points across the boundary layer and this was found to be sufficient for repeatable and reliable results.

The grid was constructed in the circular cross-section using the points of intersection of radial lines with a set of circles centred at $r = 0$. The increment in θ between successive radii was linear whereas the gap between each circle was scaled in a nonlinear fashion to improve the resolution of the boundary layers as discussed above. The radius of each mesh point was set as follows. With n points spanning the interval $0 \rightarrow r$ and thus $2n$ points in total across the toroidal cross-section, then the radius of the ith point ($i = 1, 2, \ldots, n$) is $(2r/(2n-1))((i-\frac{1}{2})^{\frac{3}{4}})$. The factor $\frac{3}{4}$ was chosen by trial and error to provide an accumulation of points near the boundary whilst maintaining an adequate coverage of the central region. It was found that a more severe factor (e.g. $\frac{1}{2}$) or a stronger rescaling required additional grid points to give a proper representation of the interior flows. These additional grid points greatly increased the computational time and so made the solution procedure impractical.

In addition to the condition of axisymmetry, the extra mirror symmetry in the two halves of the torus about the line $\theta = 0, \pi$ is imposed on the numerical solutions. Thus there is no flow allowed across this symmetry plane. This extra condition not only increases the computational speed by reducing the number of grid points but also it improves the stability of the numerical calculation.

The accuracy of the numerical scheme was checked in two different ways. First, the analytical solution of rigid-body rotation was used as an initial condition for the finite-difference scheme and this solution was found to be both stable to small perturbations and unchanged by the iteration process. Secondly, grid refinement and time-step reduction tests were carried out in order to ascertain the convergence of solutions.

In the experimental arrangement that will be discussed below, the impulsive spin-up of a torus was achieved by ramping the rotation speed from zero to its final value over

a short time. This process was modelled in the numerical calculations using a linear ramp which was a close approximation to the actual response of the physical toroidal container used in the experiments. As will be seen below, good agreement is obtained between experimental and numerical results, which gives some support to this approximation.

3. Experimental methods

The experimental apparatus and measuring techniques used to study the spin-up process are detailed in §3.1. A discussion of a novel variant of a 'phase portrait' reconstruction technique is then presented. This method enables the representation of the dynamics as trajectories in phase space reconstructed from velocity time-series measurements taken at a single point in the flow. We have adapted this technique to produce averaged phase portraits from many different experimental runs taken at the same value of C which allows us to highlight correlations between experimental runs.

3.1. *Apparatus*

The torus was formed in two halves from solid blocks of Perspex by the precision machining of a ring of semicircular cross-section in each block. The two halves were then bolted together and sealed using a rubber O-ring. All dimensions of the torus are accurate to a tolerance of 0.1 mm. The torus was filled through two small holes which were subsequently sealed using screws which were machined to the appropriate length so as not to protrude into into the flow.

The two toroidal radii are 125 ± 0.1 mm for the radius of curvature and 16 ± 0.1 mm for the cross-sectional radius, giving a radius ratio of 0.128. The torus was mounted so that it was free to rotate about its axis, as shown schematically in figure 2. As stated in the introduction, it is perhaps easiest to think of it rotating in a sense similar to that that of a bicycle wheel. A powerful servo-controlled d.c. motor was coupled to the axle via a reduction gearbox and toothed drive belt. The rotational speed of the torus was measured using an optical shaft encoder, which produed a sinusoidal wave of one hundred cycles per rotation of the axle. With this arrangement of driving motor, controller, reduction gearbox and shaft encoder the speed of the torus could be set under computer control to an accuracy of better than 0.1 %.

It is not possible to produce a sharp or instantaneous change in the speed of the torus from rest to some final value with the experimental system over the entire parameter range. Therefore, a short nonlinear ramp was used for the first 0.8 s of every run so that the torus reached its final preselected rotation rate in this time for every value of C. The use of a nonlinear ramp provided a consistent and reproducible change in speed over the whole range of interest without either overspin or oscillation in the drive. It was achieved in practice by feeding a half-Gaussian into the motor speed controller for the first 0.8 s of each run. The duration of this nonlinear ramp is less than 10% of the viscous diffusion time in the system for any of the fluids used. The form of the ramp was determined empirically and details of the procedure for selecting this particular ramp can be found in Madden (1991).

In order to cover as wide a range of C as possible we used a variety of fluids with differing viscosities to overcome the limited dynamic range of the motor and its controller. These were silicone oils of viscosity $24\ \mathrm{mm^2\ s^{-1}}$ and $5.17\ \mathrm{mm^2\ s^{-1}}$ and distilled water, which was used for the flow visualization photographs, with viscosity $1.05\ \mathrm{mm^2\ s^{-1}}$. All of the viscosities were determined using a suspended level viscometer and were measured at a temperature of 18 °C.

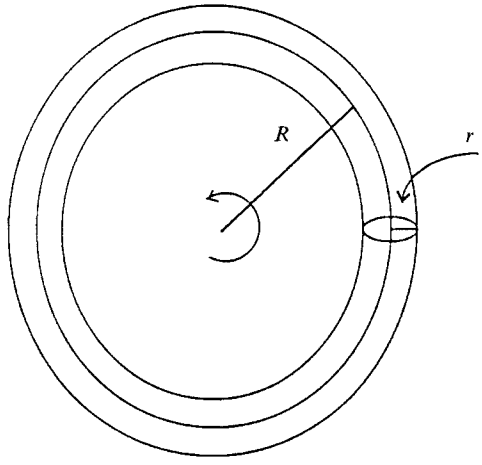

FIGURE 2. Schematic diagram of the experimental arrangement showing the principal radii of curvature.

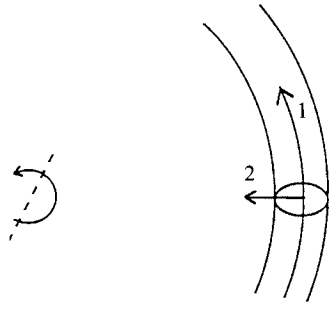

FIGURE 3. Schematic diagram shown the direction of the primary, 1, and secondary, 2, flow components.

We show in figure 3 a schematic representation of the orientation of the primary (i.e. in the direction of rotation) and secondary (towards the axis of rotation) velocity components. These fluid velocities were measured separately in different experiments using the standard technique of laser Doppler velocimetry (LDV) (see for example Drain 1980). To make these measurements, the fluid was seeded with neutrally buoyant latex spheres of diameter 1.0 μm which served as scatterers for the incident laser light. The LDV technique was employed in the differential mode and a shift frequency was applied to one of the laser beams in order to reduce the additional noise in the secondary flow measurements caused by the relatively large component of primary velocity.

In the results to be presented below, both velocity components were measured at the cross-section centre ($r = 0$). This position was chosen because of the ease and accuracy with which the optical arrangement could be aligned, given the symmetries of the torus. In addition, measurements taken at this point were found to be representative of the flow (i.e. there are no qualitative differences between measurements taken at this point and those taken at other points in the main bulk of the fluid).

Each experimental run was performed in the following way. The torus was left stationary for at least five diffusion times of the system (for the two silicone oils used, the diffusion times were approximately 10 and 50 s). The computer recording of shaft encoder and LDV signals was started and then the torus was set spinning to its required

speed using the nonlinear ramp. The torus was then left spinning until the fluid attained the rigid-body rotational state. In the experiments where primary flow measurements were taken, a fractional spin-up time was calculated from the recorded signal. This fractional spin-up time is the elapsed period between the start of the nonlinear ramp and the instant when the fluid has reached a specified fraction – in this case 95% – of the appropriate rigid-body rotational velocity.

The ramping of the input to the motor controller and the recording of signals were performed using a Masscomp computer, with its associated analog-to-digital and digital-to-analog converters. In addition to velocity measurements, flow visualization experiments were carried out. Distilled water was used which contained a flow visualization material (Mearlmaid AA natural pearl essence). The fluid was illuminated by a plane of light and photographs were taken of the spin-up process. The material reflects light in an anisotropic fashion which depends on the orientation of the particles in the flow. Thus regions of coherent orientations form light and dark patches which reveal the presence of fluid structures within the flow, see for example Savaş (1985).

3.2. *Averaging reconstructed phase portraits*

As discussed in the introduction the spin-up process can be represented by a trajectory through 'phase space'. This trajectory can be reconstructed from a velocity time-series measurement using the technique involving singular value decomposition (SVD) described by Broomhead & King (1986). The technique is, in essence, the method of delays proposed by Takens (1981) with additional analysis which provides an optimized orthonormal projection of trajectories. The method of delays and SVD can be used directly with transient data since the technique does not require stationarity of the time series.

In the present experiment, the primary flow component starts at zero velocity and ends at a value corresponding to rigid-body rotation. These two points are therefore distinct in the reconstructed phase space. In addition, the overall change in primary velocity from rest to rigid rotation is large compared with the observed velocity fluctuations, which are associated with disordered fluid motion. Therefore, it is difficult to discern some of the delicate time-dependent features using measurements of this component. The fluctuating components are, however, easily discernible using the secondary flow component which starts and ends at zero. Phase portraits were therefore reconstructed using the secondary flow velocity measurements in order to study the nature of these velocity fluctuations.

Clearly, each experimental run will furnish one portrait consisting of a single trajectory. In order to compare different runs at the same parameter values, a technique for averaging or combining phase portraits is required. The averaged phase-space portraits were produced by gluing together the time series from different runs to give one long time series. As discussed above the time series were measurements of the secondary flow velocity which in principle starts and finishes with zero value. The experimental measurements, however, contain extraneous experimental noise components which give a small offset in the measured velocity. In addition, the final value may also be non-zero because of the presence of a small amount of the primary flow component in the measurement. This effect arises because the LDV system measures the velocity component at a point in a plane. If the plane is not perfectly orthogonal to the primary flow direction, then some component of this flow will inevitably be present in the measurement. Thus, when time series from individual experiments are glued together the cumulative effect of these extraneous events results in a discontinuity between the end of one series and the start of the next. This introduces spurious steps

into the phase portraits which arise from the trajectories joining the end of one run with the start of the next. However, the number of points added is less than 5% of the total and their effect is thus small. Indeed, it is found that there is no qualitative difference between the portrait for one run and the averaged set for one hundred when the dynamics of the flow are repeatable.

4. Results

The experimental and numerical results presented in this section describe the changes in the spin-up process of the fluid which arise from increasing the final rotation rate of its toroidal container. The results are therefore discussed with reference to the non-dimensionalized form of the control parameter C. We first present in §4.1 an overview of the experimental and numerical results for the entire range of C covered. It is observed that the qualitative nature of the results is the same over ranges of C with definite end points to each span. Thus the ensuing discussion is arranged in order of increasing C and each type of behaviour is described in sequence. In §4.2 the value of C is generally less than 1000, the fluid motion is axisymmetric and it is found that there is good agreement between the numerical and experimental results. Over the next range of C, discussed in §4.3, three-dimensional transient wave phenomena are observed. Here values of the parameter C are greater than 1000 and differences between the experimental and numerical results begin to appear as the limits of the theoretical approximations are reached. Therefore, greater emphasis is placed on the experimental results in this regime. Finally, the waves are found to grow and break with further increase in C so that turbulence now forms part of the spin-up process.

The experimental results are presented in several forms. These are time series measurements, graphs of fractional spin-up time versus C, reconstructed phase portraits and flow visualization photographs. The numerical results consist of fractional spin-up times, secondary flow distributions and velocity time-series measurements for one of the central grid points. A combination of all of the results is used to demonstrate the sequence of dynamical fluid states that appear as the final rotational rate is increased and that arise because of the hydrodynamic instabilities in the spin-up process of the fluid.

4.1. *The trend in fractional spin-up time as a function of C*

We begin the discussion of the results by considering the fractional spin-up time of the flow over the entire range of C studied. A log–log graph of this quantity is shown plotted against C in figure 4. As defined in §3.1, the non-dimensionalized fractional spin-up time is the elapsed period between setting the toroidal container in motion and the instant when the primary fluid velocity has reached 95% of its solid-body rotational value. We choose to use the non-dimensionalized time discussed in §2.2 to ease comparison between the theoretical and experimental results. The numerically obtained results are only valid for a limited span of C but we have linearly extrapolated them over the entire range to highlight the departure of the experimental results from the numerical results. This extrapolation is shown by the solid line CD.

In the range of C between 10 and approximately 30 ($\log C$ between 1 and 1.5) the spin-up process is dominated by viscous diffusion of vorticity from the walls. Further, if we assume that secondary flow effects due to curvature are negligible in this limit of small C then we may approximate the situation by considering it to be equivalent to the starting motion in a long straight pipe which is suddenly accelerated from rest. Straightforward adaptation of a model problem given in chapter 4.3 of Batchelor

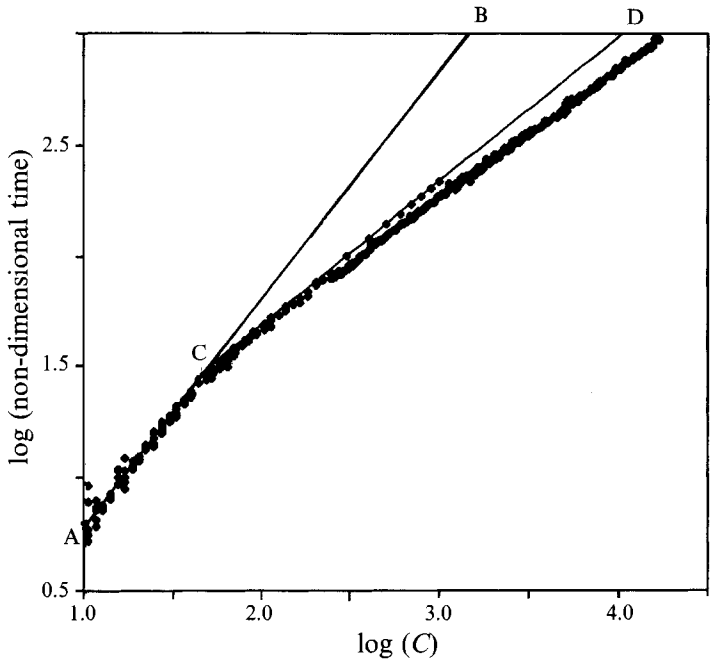

FIGURE 4. The combined theoretical, numerical and experimental results showing the logarithm of the non-dimensionalized spin-up time as a function of C. AB is obtained from the analytical result for the start-up flow of a long straight pipe and CD is the best-fit line through the numerical results in the upper range of C.

(1967) shows that the scaling of the ensuing solution will proceed as $r^2/2\nu t$. Thus an analytical estimate of the spin-up time can be obtained and since a similarity solution exists then this will be independent of C. This is shown as the line AB in figure 4 which has a slope of 1 since we have used the non-dimensionalized time to construct this figure. It can be seen that there is excellent agreement between theoretical, numerical and experimental results up to the point labelled C in figure 4.

In the range of C between 30 and 250 ($\log C$ between 1.5 and 2.4) the spin-up time becomes dependent on C as secondary flow effects become important. Now there is very good agreement between the numerical and experimental results which is an indicator that the flow remains axisymmetric throughout the spin-up process. The line CD is a straight-line fit to the numerical results at the upper end of this range of C and it has a slope of 0.647 showing that secondary flow is a significant factor in enhancing the spin-up process.

It may be seen in figure 4 that there is a difference between the experimental and numerical results above $C \approx 250$ ($\log C \approx 2.4$). This is because three-dimensional effects become important and these are not included in the numerical approximation. However, the experimental results scale in proportion to $\log C$ and the least-squares fitted line has a slope of 0.641. Thus it can be seen that the complicated motions which arise in this range of C and which will be discussed in detail below do not have a significant effect on the spin-up time. This is an interesting and perhaps surprising result since complicated motions including transient turbulence can form part of the process over a large part of this range of C. Since turbulence enhances the transport of vorticity one might expect its presence to have a significant effect on the spin-up time. However, the final state is that of solid-body rotation and so the turbulence must

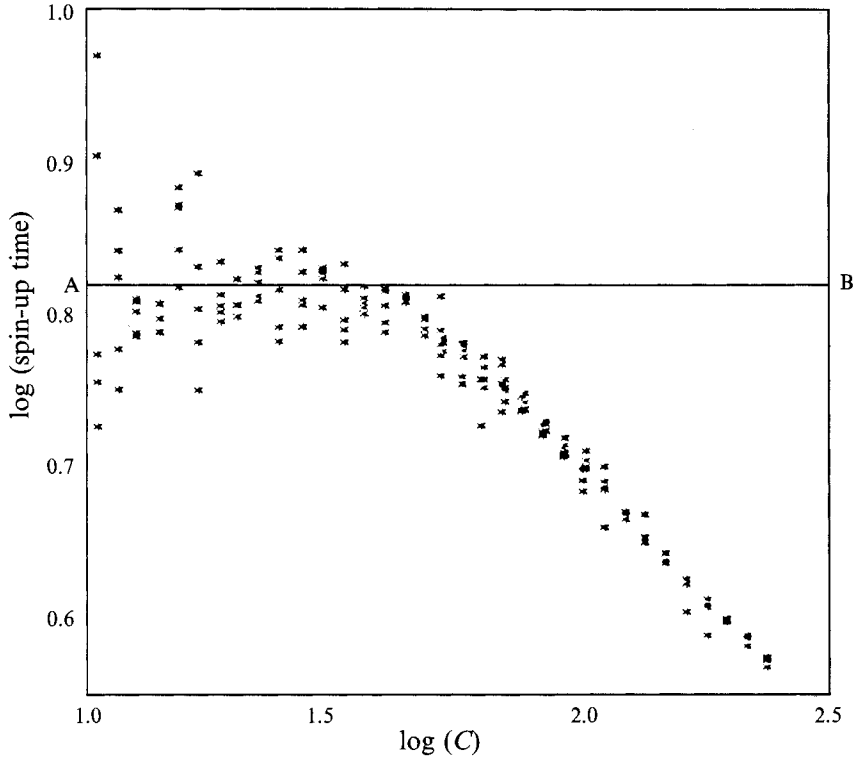

FIGURE 5. Log–log plot of the experimentally determined dimensional spin-up time plotted as a function of C for the lower range of C studied. Note how it is independent of C up to log $C \approx 1.5$.

also decay. Thus one conclusion which may be drawn from the present results is that the two effects approximately cancel each other out.

4.2. *Experimental and numerical results for C less than* 1000

At small values of C the spin-up time is independent of C as discussed in §4.1 above. Here, the spin-up process is dominated by viscous diffusion of vorticity from the walls of the torus, and the flow is almost entirely in the primary, rotational direction with little or no secondary flow. The independence of the spin up time of C is demonstrated by the horizontal portion of figure 5 between C values of 10 and 30 ($\log C$ values of 1 and 1.5). Here we have chosen to plot the dimensional time since the independence of this measure of C is more immediately evident. We also show for comparison the analytical estimate of the spin-up time which is denoted by the horizontal line AB. In the region where C is approximately 10, the signal-to-noise ratio is poor in the experimental results owing to problems with the LDV technique when measuring small velocity components. Consequently there are large errors associated with the experimental estimates of the spin-up time but on average there is good agreement between calculation and experiment.

When C is increased above this linear range, secondary flow effects become important, and for C greater than 30 ($\log C \approx 1.5$), the spin-up time is no longer independent of C. The transport of vorticity from the boundary is now enhanced by the action of secondary flow which reduces the fractional spin-up time to a value below that which would be achieved by viscous diffusion alone. The growth of the secondary

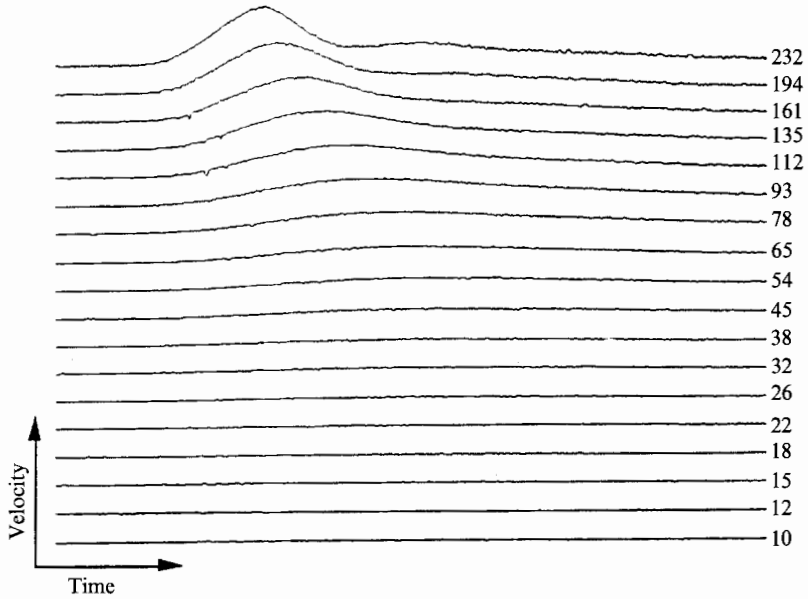

FIGURE 6. Plots of the measured secondary flow component as a function of time. Each plot is for a different value of C as labelled, and each line is 5 s of data.

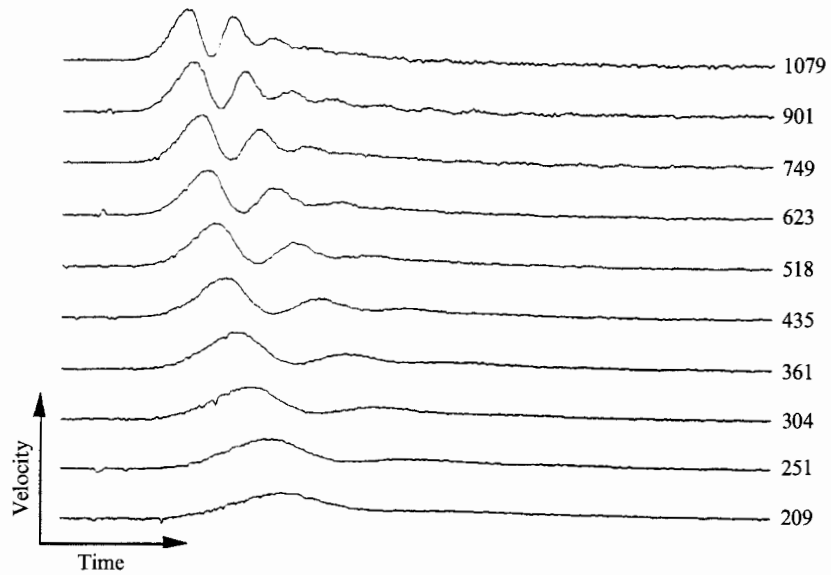

FIGURE 7. Plots of the measured secondary flow component as a function of time. Each plot is for a different value of C as labelled and each line is 5 s of data. The development of an inertial oscillation is clear.

flow component is shown clearly in figure 6, in which a sequence of experimental velocity time series for a range of C is shown. The parameter C is varied from 10 at the bottom to 232 at the top, which covers the range shown on the x-axis of figure 5. It should be noted that the peak amplitude for the secondary flow component is less than 10% of the primary component in this regime.

Next we show in figure 7 the observed sequence of secondary flow time series when C ranges from 209 to 1079. It can be seen that the secondary flow develops an

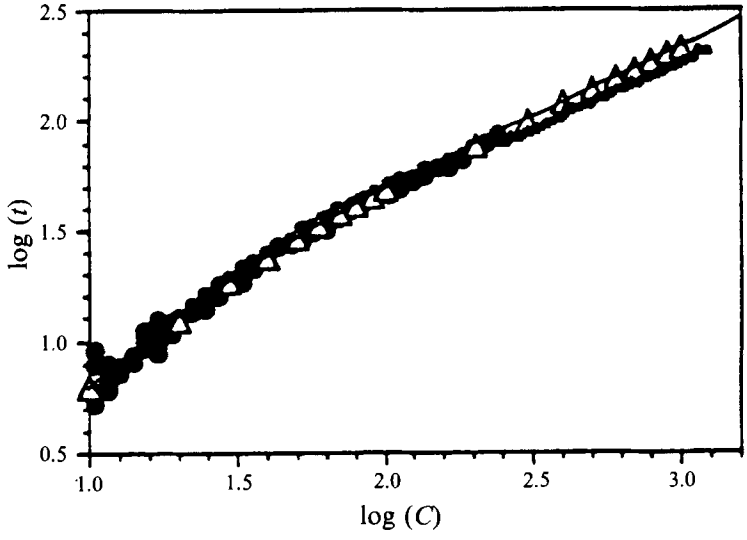

FIGURE 8. Detailed comparison of the experimental and numerical results for non-dimensionalized spin-up time shown on a log–log scale: ●, 0.24 Cst Silicone oil; ▲, 0.0517 Cst Silicone oil; △, numerical (with cubic fit).

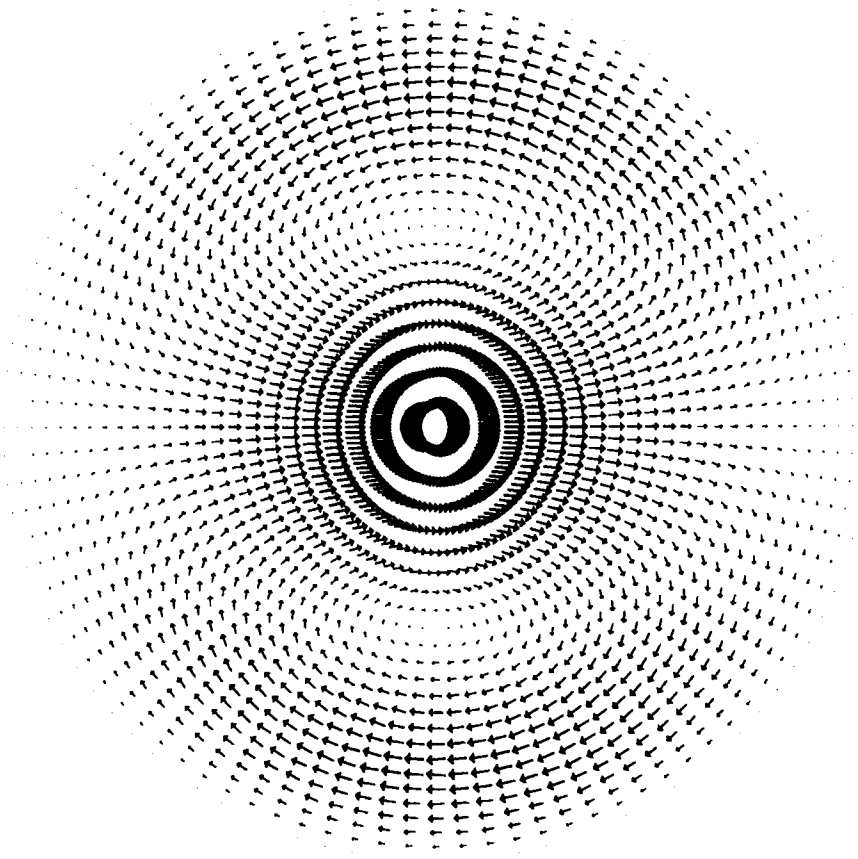

FIGURE 9. Calculated secondary flow pattern which is typical of that found during the spin-up process. Here $C = 75$ and elapsed time is 2.3 s after start.

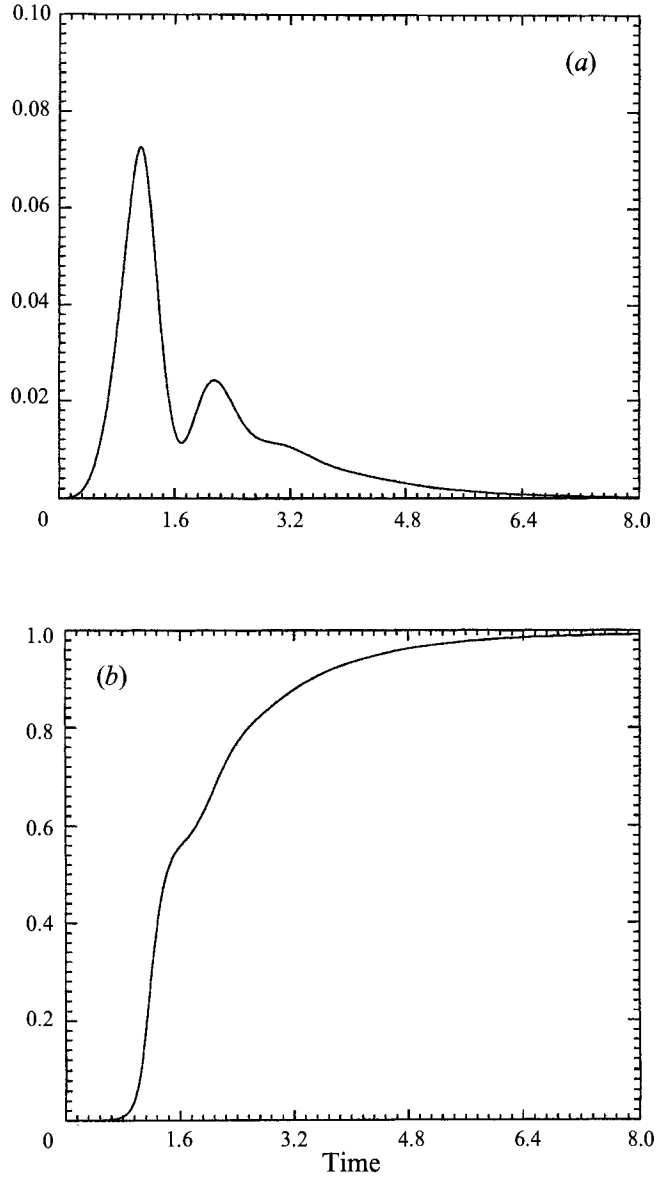

FIGURE 10. Calculated velocity time series for $C = 300$: (*a*) the secondary flow component, and (*b*) the primary. The duration of the record is 8 s.

oscillation which is at twice the rotational frequency. Inertial oscillations of this type are well-known phenomena in spin-up problems, and are discussed by Greenspan (1968). A comparison between the experimentally and numerically determined non-dimensionalized spin-up times for this range of C is presented in figure 8. This figure has been constructed from two sets of experimental data, each with a fluid of different viscosity, and the numerically calculated set. In order to allow a direct comparison the spin-up time has been non-dimensionalized using the scaling parameters described in §2. The independence of fractional spin-up time of C is therefore indicated in this figure by the line of slope 1 which occurs for $\log C$ less than 1.5 ($C \approx 30$). The agreement between experimental and numerical values is generally very good and the two sets of

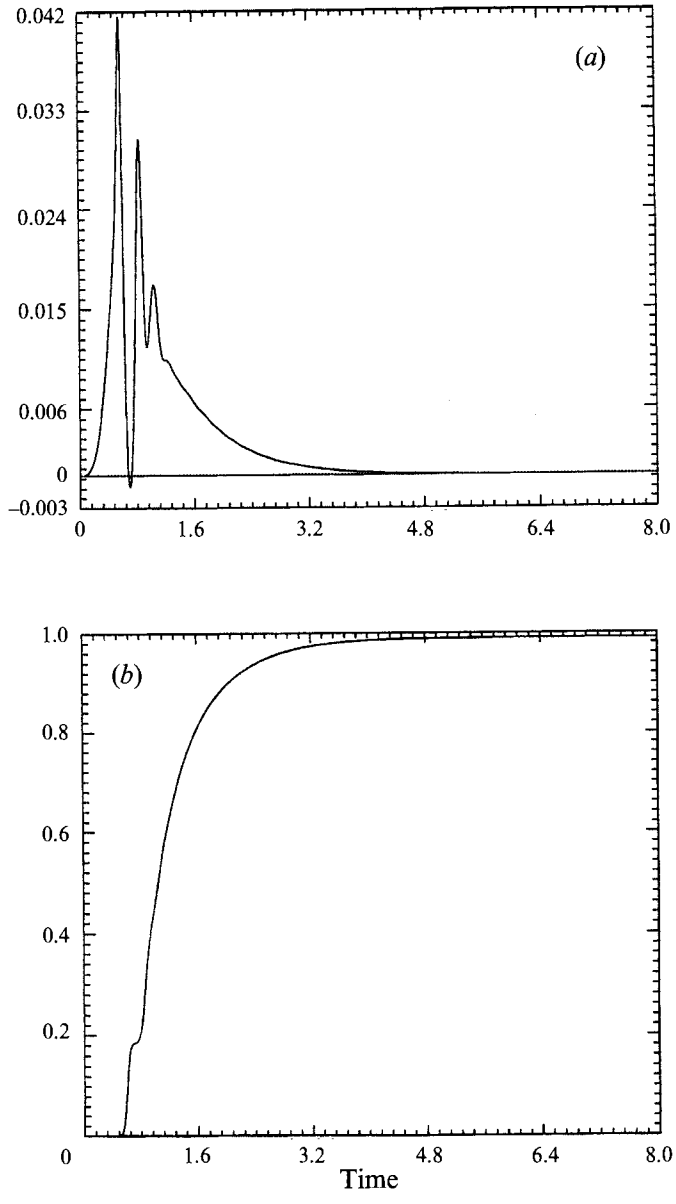

FIGURE 11. Calculated velocity time series for $C = 1500$: (*a*) the secondary flow component, and (*b*) the primary. Note the reversal in the secondary flow component (*a*).

results are coincident for $\log C$ less than 2.5 ($C \approx 300$). However, for values of $\log C$ greater than 2.5 there are differences between the two which develop with increasing C and which become approximately 3% of the spin-up time for each value of C. To highlight this difference we have fitted lines to the experimental and numerical data for this region, using standard least-squares techniques, and it is found that the gradients differ by more than 6%, indicating a divergence of the numerical and experimental spin-up times. As discussed in §4.1 this divergence is probably due to the appearance of three-dimensional phenomena in the experiment as well as the lack of numerical resolution of the boundary layers.

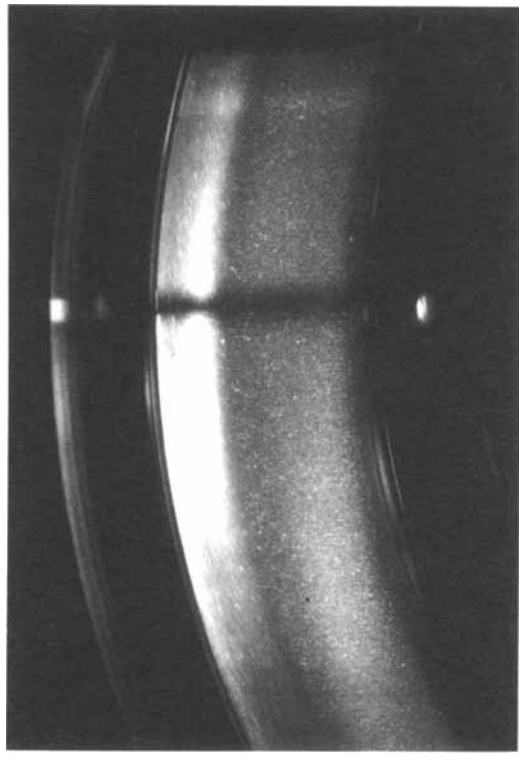

FIGURE 12. Flow visualization photograph taken 2 s after start with $C = 1257$.

We now show in figure 9 a typical numerically determined secondary flow pattern for the above range of C. Here the axis of rotation is to the right of the page and fluid moves away from this axis when adjacent to the wall and towards it in the centre of the torus. We have represented the flow by arrows centred at each grid point and their size and orientation indicate the magnitude and direction of the velocity at that grid point. The two counter-rotating vortices shown in this figure are similar to those found in pressure-driven flow through curved pipes but as discussed in the introduction their rotation is in the opposite sense here. This secondary flow pattern is only a transient phase and it will eventually be removed by the action of viscosity as solid-body rotation is achieved.

The inertial oscillations which are observed in the experiment and illustrated in the time series of figure 7 are also reproduced by the numerical calculations. We show in figure 10 a numerically derived time series for $C = 300$. Here both primary and secondary flow velocities at one of the central grid points are portrayed as a function of time. The vertical scale is the same in each picture and it has been normalized by the maximum value of the primary velocity in the centre of the torus cross-section. Hence the primary flow component at the cross-section centre changes from 0 to 1 during spin-up. The time series shown has a total length of 8 s and in this time both the secondary and primary flows reach their final values – zero and 1 respectively. The inertial oscillations which were discussed above with reference to figure 7 are clearly visible in the secondary flow time series of figure 10.

As the value of C is increased beyond the upper limit of the range of figure 5, the numerically determined spin-up times and the experimental values diverge as discussed above. At the same time, the numerical solution develops a transient four-vortex

FIGURE 13. Flow visualization photograph taken 2 s after start with $C = 2513$.

secondary flow. Here, not only are there two counter-rotating vortices similar to those of figure 9, but in addition, a smaller second vortex pair exists near the centre of the cross-section.

A velocity time series generated from the numerical integrations for this four-vortex solution is portrayed in figure 11. The secondary flow, which is once again shown overlaid on the primary flow with a shifted and magnified scale, now contains evidence for flow reversal as well as displaying the inertial oscillations discussed above. The four-vortex state occurs at the minimum (i.e. most negative) value for this secondary flow. As discussed in the introduction four-vortex states have been calculated and observed for oscillating flows in curved pipes in the high-frequency limit by Lyne (1970). However, Lam (1988) has shown that the flow that arises in an impulsively started pipe is susceptible to boundary-layer collision and separation. The collision and separation processes may result in the four-vortex state being unstable and thus it is not observed in the experiment. Further evidence for these instabilities will be presented in the next section.

4.3. *Experimental results for C greater than* 1000

The photograph shown in figure 12 was taken with an exposure time of 1/30th of a second so that it is effectively an 'instantaneous' flow visualization realization of the flow field at $C = 1257$ after an elapsed time from the start-up of approximately 2 s. The fluid is illuminated by a plane of light along the centreline of the cross-section perpendicular to the axis of rotation. This axis is to the right of the page and the torus would then be rotating in the plane of the paper in this geometry. The flow field shown

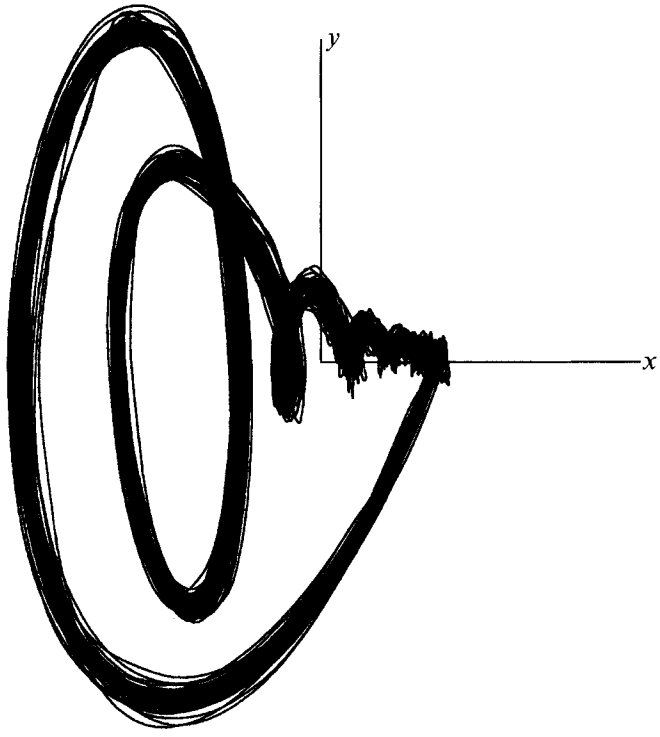

FIGURE 14. Reconstructed phase portrait for $C = 1215$. Here the time series from 50 independent runs have been used in the construction. The data have been projected onto the three principal singular vectors calculated by the SVD of the constructed trajectory points whose coordinates are time-delayed values of velocity.

in the photograph is representative of the spin-up process for values of C between approximately 1000 and 2500. The dark horizontal band is a shadow cast by a mounting bolt outside the fluid-filled toroidal cavity. Inspection of the photograph reveals a sharp interface between rotating fluid on the left and stationary fluid on the right. This front is axisymmetric at all times and progresses across the torus from left to right with increasing experimental run time. These sharp fronts are beyond the resolution of the numerical calculations and may be related with the boundary-layer collision processes discussed by Cowley *et al.* (1990) and Lam (1988).

When C is increased further, the interface shown in figure 12 becomes unstable and loses its axisymmetry. This breaking of the axisymmetry was observed to occur for C values approximately equal to 2500 using flow visualization. A typical flow visualization photograph for this regime is shown in figure 13 where $C = 2513$. As in figure 12, there is a boundary between stationary and rotating fluid. However, it is evident in the photograph that this front is no longer axisymmetric as there are several dark streaks or waves along its leading edge. We believe that these waves originate at the centrifugally unstable region near the inner wall and are then convected round the outer wall of the torus by the secondary flow field. They then travel back towards the inner wall across the middle of the tube and, since they are growing during their passage, first become visible on the leading edge of the front.

We now turn to a dynamical-systems representation of the flow dynamics to explore the three-dimensional instabilities described above in more detail. The velocity time series obtained from the LDV system can be used to construct individual trajectories

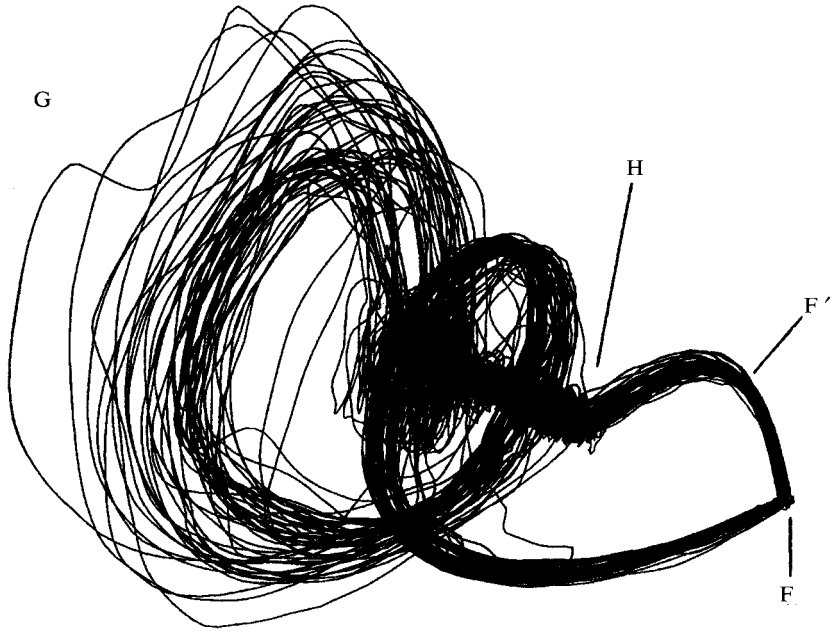

FIGURE 15. Reconstructed phase portrait for $C = 3403$. Here the time series from 100 independent runs have been used in the construction. The trajectories start at the point labelled F, remain together initially and then diverge wildly around the region labelled G before they converge in the nearly fully spun-up state labelled H. The data have been projected onto the three principal singular vectors calculated by the SVD of the constructed trajectory points whose coordinates are time delayed values of velocity.

through a reconstructed phase space using the techniques described in §3.2. In this representation each trajectory corresponds to an individual spin-up process. Thus an accumulation of many such runs will give rise to a phase-portrait representation of the dynamics involved in the spin-up process. Examples of these phase portraits are given in figures 14 and 15. The three axes onto which we have projected the data are velocity and two time-delayed values of velocity for different but constant time delays. The projected data have then been processed using the singular systems approach discussed by Broomhead & King (1986).

The phase portrait in figure 14 is formed from fifty separate runs at a value of C set equal to 1215. It can be seen that, despite the fact that the fluid motion is non-trivial, the phase trajectory is well-defined, i.e. the paths stay close together at all times and are only separated by experimental noise. However, non-uniqueness in the spin-up path is demonstrated in the phase portrait shown in figure 15 which has been constructed from 100 separate runs at $C = 3403$. The portion marked F′ is caused by the spurious points introduced in connecting the end of one run with the start of the next, as discussed in §3.2. The time evolution of the trajectories proceeds as follows. All the trajectories start at the point labelled F and move outwards through G, before spiralling into the point H. Initially the trajectories progress closely together but then their paths diverge before converging once more to the final state. Thus the trajectories follow different paths through the reconstructed phase space for the same initial conditions.

The non-uniqueness discussed above can also be seen in the time-series plots of the secondary flow as shown in figure 16. This feature has the form of a disturbance which grows in amplitude and duration as C is increased from the transition value of

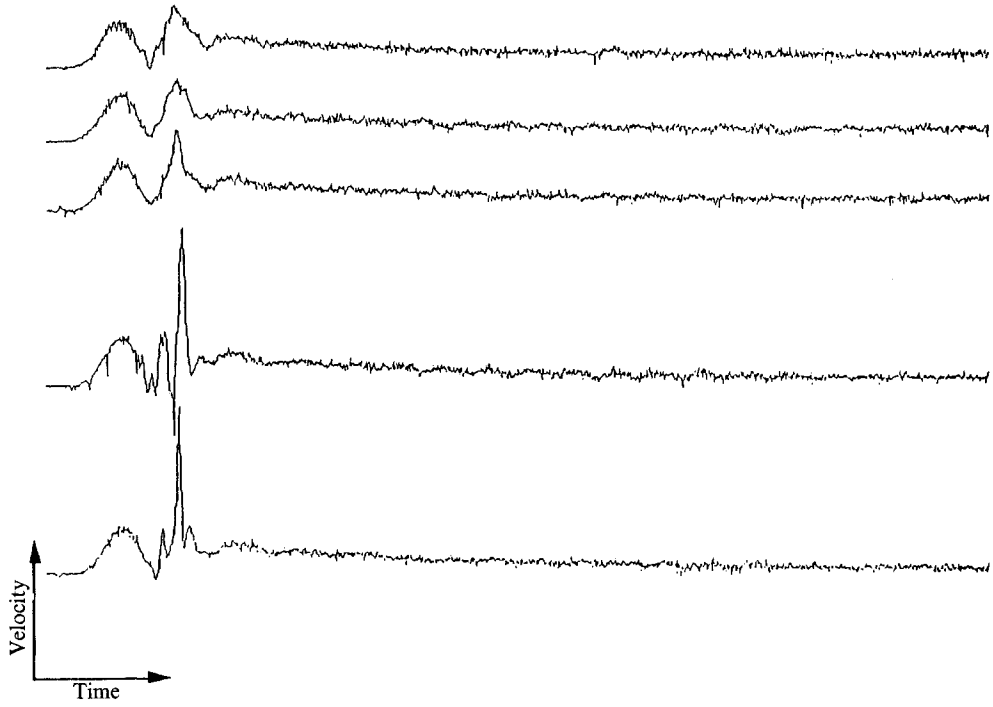

FIGURE 16. Velocity time series plots for $C = 3038$ which show the first signs of non-uniqueness. Each record is 6 s long and were obtained from five repeat runs of the experiment.

approximately 2650. The five time series plots for $C = 3038$ given in figure 16 show a variety of these disturbances which include some sharp singular-type events. Next, the flow visualization photograph of figure 17 shows the result of nonlinear developments of the waves on the front when C is increased to 3770. Here, it can be seen that the original axisymmetric front of figure 12 has now broken up and is highly irregular.

A new phenomenon appears with yet further increase in the value of C. This can best be seen by inspection of figure 18 which contains ten secondary flow time series with $C = 5345$. Now there is a second distinct disturbance which arises after the initial one discussed above has decayed. This second disturbance is observed above $C \approx 4800$, and it is associated with the appearance of a wave on the front which develops from the inner wall. The initial formation of this new front is portrayed in the sequence of flow visualization photographs of figure 19(*a–d*). The development of a wave on the front near the inner wall is clearly visible in the photographs. This wave subsequently grows and then breaks down into highly disordered flow. This new phenomenon is associated with a kink in the plot of spin-up times versus C at $C \approx 5000$ ($\log C \approx 3.7$). We show a magnified version of this particular feature in figure 20 which is constructed from approximately 600 individual experimental runs. A similar kink is observed in the plot of spin-up time versus C for the transition between axisymmetric and non-axisymmetric flows. In both cases however the kinks appear as small disturbances in the overall trend, which indicates that the spin-up time is an insensitive measure of the dynamical-fluid state as can be seen by inspection of figure 4.

Finally, the time series plots shown in figure 21 which were taken at $C = 7163$ indicates that, as C is increased, the initial and secondary disturbances merge and the scale of the combined disturbance grows. In addition, the phase-space projection for

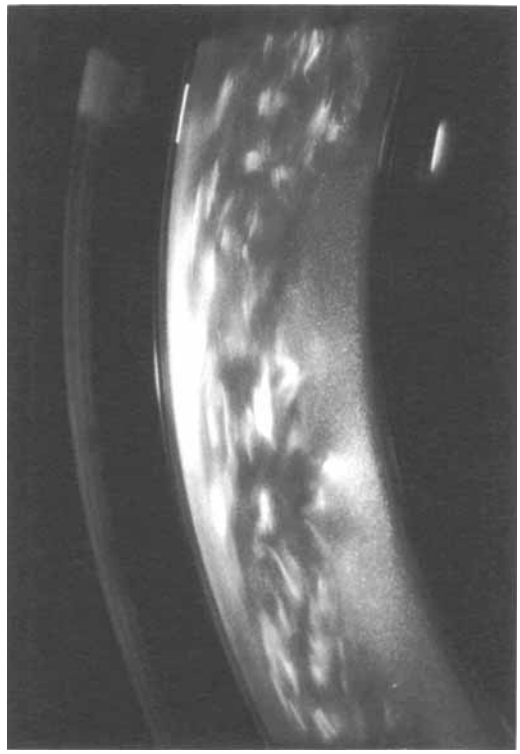

FIGURE 17. Flow visualization photograph taken with $C = 3770$ showing the final stages of the break-up of the front.

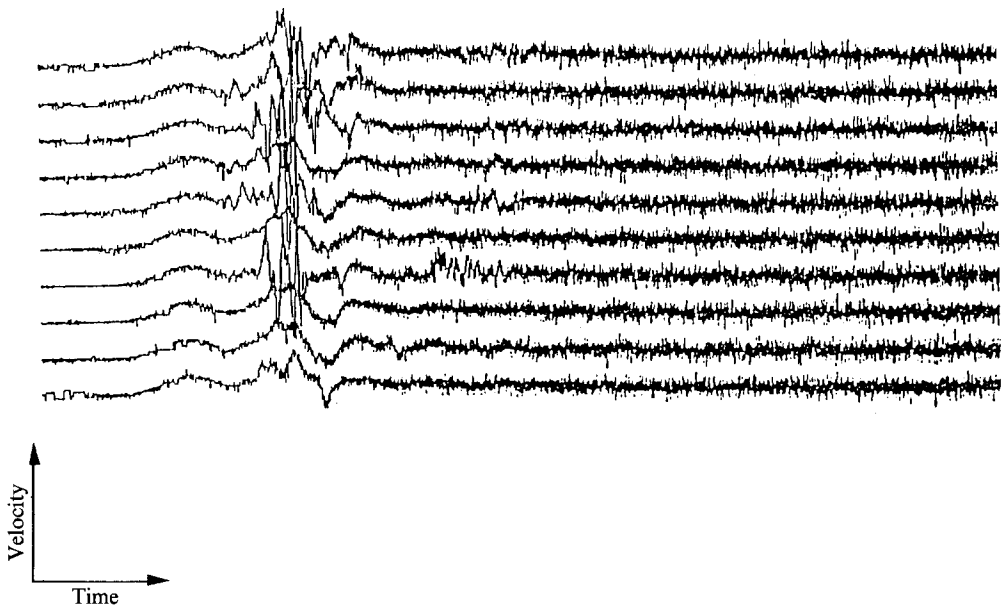

FIGURE 18. Ten velocity time series for the radial flow component taken at $C = 5354$ chosen to highlight the unrepeatability of the flow dynamics in the spin-up process at high values of C.

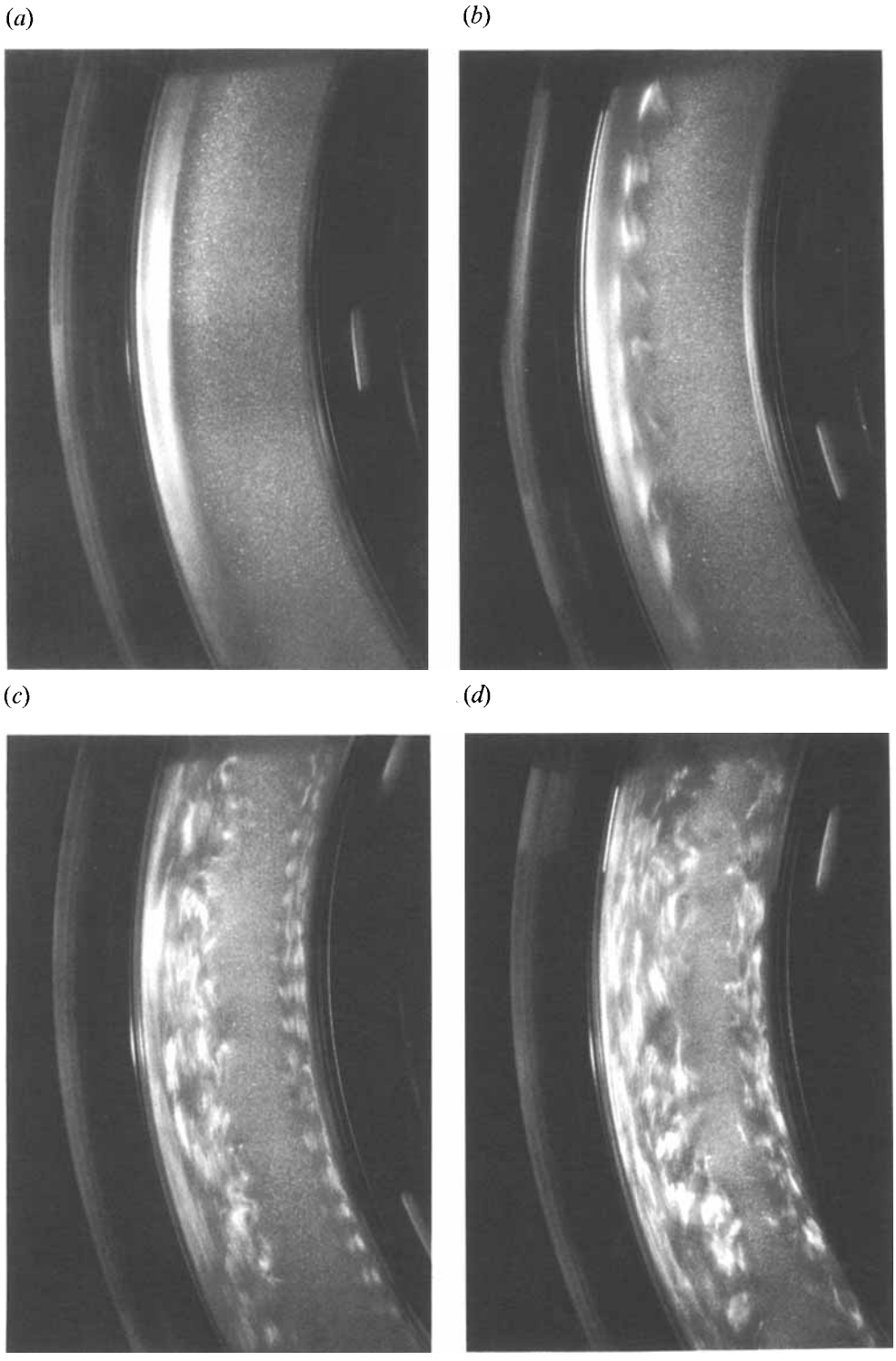

FIGURE 19. Sequence of flow visualization photographs showing the development of the flow instabilities during the spin-up process at $C = 7540$. The elapsed times after the start of the container are (*a*) 0.5 s, (*b*) 0.75 s, (*c*) 1.0 s, and (*d*) 1.25 s.

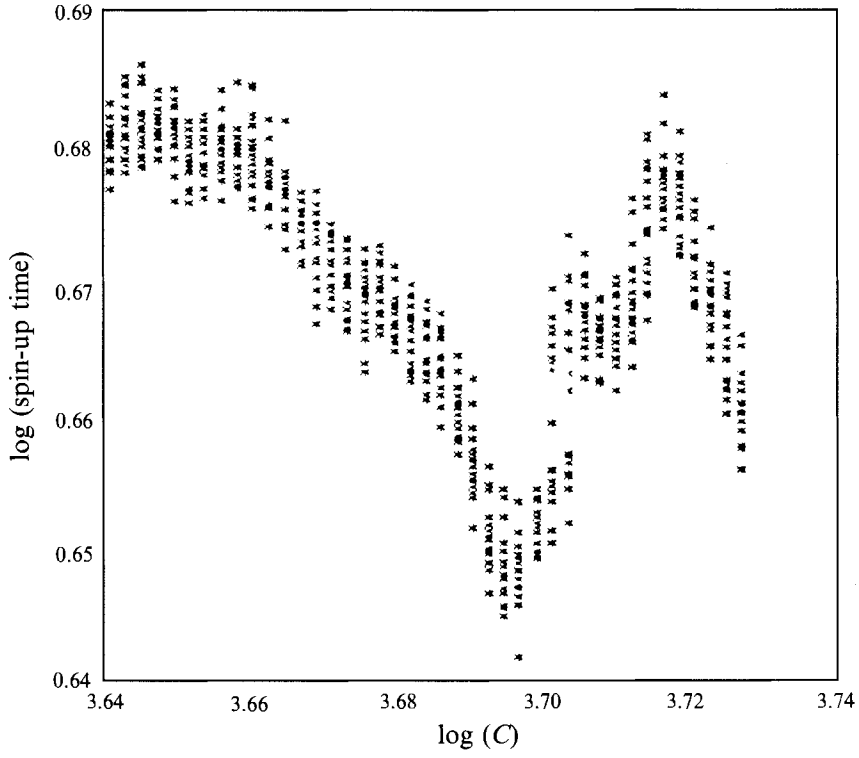

FIGURE 20. Plot of dimensional spin-up time versus C showing the kink in the curve corresponding to the appearance of a fluid instability. The data from approximately 600 runs were used to construct this figure.

$C = 7146$, which contains trajectories from *two* runs, is shown in figure 22. Here the trajectories from different runs diverge, wandering wildly, before eventually converging on the rigid rotational state. There is now no obvious low-dimensional dynamical structure associated with the spin-up process.

5. Conclusions

A combination of numerical and experimental techniques has been used to uncover a rich variety of interesting dynamical behaviour in the spin-up of a fluid in a toroidal container. The transient phase between rest and solid-body rotation has been studied by varying the final rotation rate, which we have non-dimensionalized and defined as C. At small values of C momentum is transported from the walls of the container to the fluid by the action of viscous diffusion. The spin-up process is then enhanced by the action of secondary flows at higher rates of rotation and the transient flow is axisymmetric in both of these regimes. Further, good agreement is found between the experimental and numerical results, including the development of inertial oscillations.

In the next range of rotation rate the flow becomes three-dimensional so that the numerical model is no longer valid. This breaking of axisymmetry is accompanied by the observation of fronts which eventually break down into transient disordered flow with increase in C. We speculate that there are two possible processes involved in the formation and break-up of the observed fronts. The first of these is a boundary-layer collision process of the type studied theoretically by Cowley *et al.* (1990). However, the

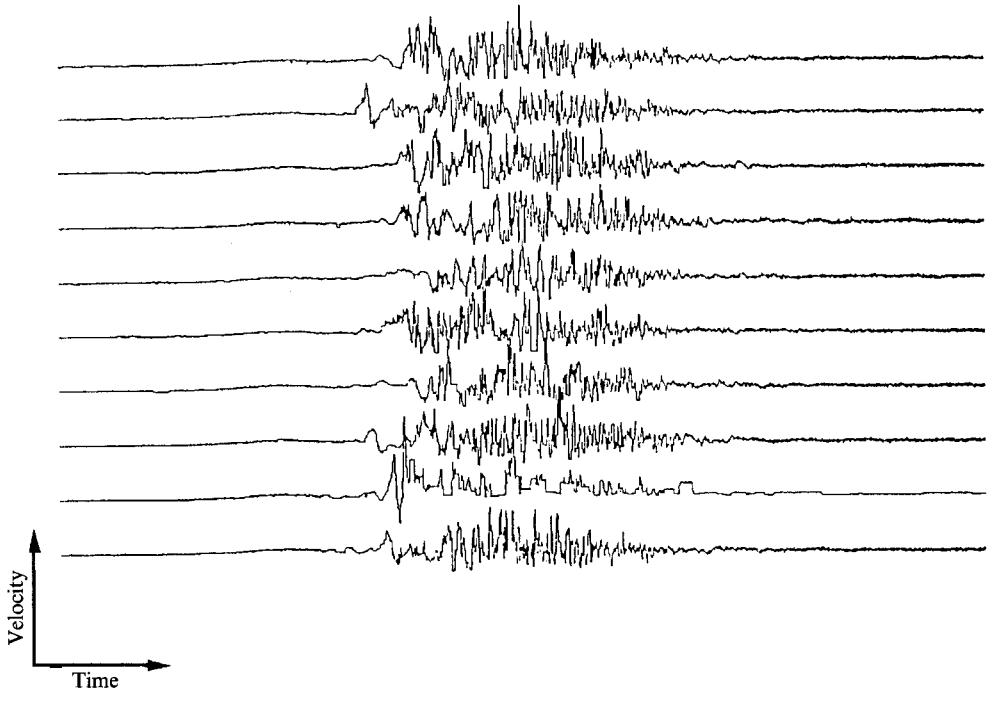

FIGURE 21. Ten velocity time series plots taken at $C = 7163$ showing transient turbulent phase.

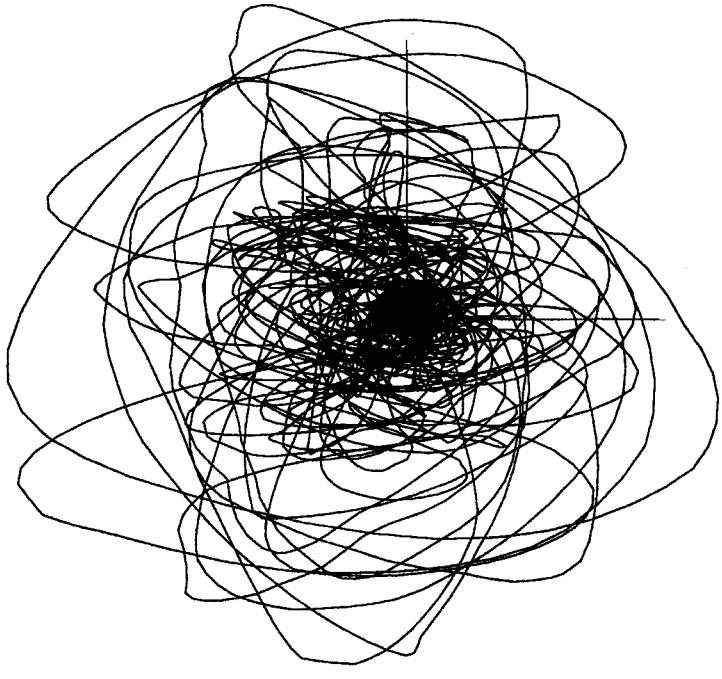

FIGURE 22. Reconstructed trajectories from two separate runs taken at $C = 7146$. The data have been projected onto the three principal singular vectors calculated by the SVD of the constructed trajectory points whose coordinates are time-delayed values of velocity.

problem they studied was the physically unrealistic situation where the velocity of the boundary was instantaneously set to a large finite value. In our experiments, the container is ramped to the final value so that reproducible changes in the parameter C can be realized over the entire parameter range. The collision process studied by Cowley *et al.* would occur within the timescale of the initial stages of ramp and so a direct comparison cannot be made. Nevertheless, we would expect some features of collision processes to be retained and thus the observed front may be a remnant of the boundary-layer collision.

The second source of the wavefronts is the following. The primary flow is centrifugally unstable near the inner wall as the circulation decreases outwards there. Thus instabilities should appear there but they will require some time to grow. Also present is a secondary flow component which would convect any instabilities formed near the inner wall circumferentially around the minor radius of the torus. They would then be carried across the diameter in the cross-section of the torus from the outer towards the inner wall. During this convective phase the instabilities would have time to grow so that they would appear as waves on the front and be stretched by the action of the strong local shear. In addition, at the upper end of the range of C the inner wall shear is much sharper and so the instability can grow much more quickly. Thus in this case an instability is observed on both walls with the outer one appearing first. Both of these instabilities eventually grow nonlinearly to produce highly disordered flow which could be described as transient turbulence.

We have shown that the spin-up process is well defined and repeatable over a range of C that is delimited by a critical event at either end. This is somewhat analogous to a sequence of bifurcations in for example the Taylor–Couette system as the Reynolds number is varied. The transitions between each of the states is signified by changes in the slope of the plots of spin-up time against final rotation rate. However, these discontinuities in the slope are small yet distinct features and the overall trend in the spin-up time is dominated by secondary flow effects. Perhaps one surprising feature of this is that the creation of transient turbulence does not have a marked effect on the spin-up process. This is because once the turbulence has appeared it takes some finite time to decay and there appears to be an overall balance in the two processes. More recently, it has been suggested that the results of a study of the decay of turbulence in this system may be compared with analytical scaling arguments (C. Foias, private communication).

Finally we considered the spin-up, process from a 'dynamical systems' point of view in an attempt to classify the observed dynamical behaviour. The two end points of the process, rest and rigid-body rotation, can be considered as distinct points in solution space and the transient phase as a trajectory through the space. We have used nonlinear signal processing techniques to reconstruct the phase space using single-point velocity measurements and shown that the trajectory is unique up to the stage when the non-axisymmetric fronts first develop. A saddle then appears in the phase space where trajectories which initially follow similar paths diverge from each other so that their total paths through phase space are non-unique. This is a definite critical event in the transient behaviour and we have attempted to calculate the local dimension of the attractor on either side of this critical point. To date, however, we have been frustrated by the lack of resolution of the data and noise. Nevertheless this approach has clarified the systematic nature of the dynamics of this transient process.

The authors are grateful to the SERC who supported this research through the 'Nonlinear Initiative' and through and 'Instant Studentship' (F.N.M). Keith Long

rose to the challenge of manufacturing the high-precision torus with great aplomb. The original idea for this project came from a misheard idea of Ciprian Foias, although the final version was much closer than any of us suspected. The authors benefitted from discussions with S. J. Cowley, C. Foias and S. J. Hogan.

REFERENCES

BATCHELOR, G. K. 1967 *An Introduction to Fluid Dynamics*. Cambridge University Press.

BENTON, E. R. & CLARKE, A. 1974 Spin-up. *Ann. Rev. Fluid Mech.* **6**, 257–280.

BERGER, S. A., TALBOT, L. & YAO, L.-S. 1983 Flow in curved pipes. *Ann. Rev. Fluid Mech.* **15**, 461–512.

BERTELSEN, A. F. & THORSEN, L. K. 1982 An experimental investigation of oscillatory flow in pipe bends. *J. Fluid Mech.* **118**, 269–284.

BROOMHEAD, D. S. & KING, G. P. 1986 Extracting qualitative dynamics from experimental data. *Physica* **20D**, 217–236.

COWLEY, S. J., VAN DOMMELEN, L. L. & LAM, S. T. 1990 On the use of Lagrangian variables in descriptions of unsteady boundary-layer separation. *Phil. Trans. R. Soc. Lond.* A **333**, 343–378.

DEAN, W. R. 1928 The streamline motion of fluid in a curved pipe. *Phil. Mag.* **5**, 673–695.

DRAIN, L. E. 1980 *The Laser Doppler Technique*. John Wiley and Sons.

GREENSPAN, H. P. 1968 *The Theory of Rotating Fluids*. Cambridge University Press.

GREENSPAN, H. P. & HOWARD, L. N. 1963 On a time-dependent motion of a rotating fluid. *J. Fluid Mech.* **17**, 385–404.

IBRANI, S. & DWYER, H. 1987 Flow intractions during axisymmetric spin up. *AIAA J.* **25**, 1305–1311.

LAM, S. T. 1988 On high Reynolds number laminar flows through a curved pipe and past a rotating cylinder. PhD thesis, University of London.

LYNE, W. H. 1970 Unsteady viscous flow in a curved pipe. *J. Fluid Mech.* **45**, 13–31.

MADDEN, F. 1991 Dynamical instabilities in a fluid spin-up and in an open flow system. DPhil thesis, University of Oxford.

MULLIN, T. 1993 *The Nature of Chaos*. Oxford University Press.

MUNSON, B. R. 1976 Secondary flows in a slowly oscillating torus. *Phys. Fluids* **19**, 1823–1825.

PEARSON, C. E. 1967 A numerical study of the time-dependent viscous flow between two rotating spheres. *J. Fluid Mech.* **28**, 323–336.

PRESS, W. H., FLANNERY, B. P., TEUKOLSKY, S. A. & VETTERLING, W. T. 1988 *Numerical Recipes in C*. Cambridge University Press.

SAVAŞ, Ö. 1985 On flow visualization using reflective flakes. *J. Fluid Mech.* **152**, 235–248.

TAKENS, F. 1981 *Detecting Strange Attractors in Turbulence*. Lecture Notes in Mathematics, (ed. D. A. Rand & L. S. Young) Springer.

TRITTON, D. J. 1988 *Physical Fluid Dynamics*, 2nd edn. Oxford University Press.

WATKINS, W. B. & HUSSEY, R. G. 1977 Spin-up from rest in a cylinder. *Phys. Fluids* **20**, 1596–1604.

WINTERS, K. H. 1987 A bifurcation study of laminar flow in a curved tube of rectangular cross section. *J. Fluid Mech.* **180**, 343–369.

YAVORSKAYA, I. M., BELYAEV, Y. N., MONAKHOV, A. A., ASTAF'EVA, N. M., SCHERBAKOV, S. A. & VVEDENSKAYA, N. D. 1980 Stability, non-uniqueness and transition to turbulence in the flow between two rotating spheres. In *Proc. XV Intl Congr. of Theoretical and Applied Mechanics.*